VHF-ST Radar Observations of an Upper-Level Front Using Vertical and Oblique-Beam C_N^2 Measurements

J.-L. CACCIA

Laboratoire de Sondages Electromagnétiques de l'Environnement Terrestre, Université de Toulon et du Var, La Garde, France

J.-P. CAMMAS

Laboratoire d'Aérologie, Université Paul Sabatier, Toulouse, France

(Manuscript received 3 December 1996, in final form 30 April 1997)

ABSTRACT

Mesoscale aspects of an upper-level front that moved over Brittany (France) during the Mesoscale Frontal Dynamical Project 1987 experiment are investigated using very high frequency stratospheric–tropospheric (VHF-ST) radar data and European Centre for Medium-Range Weather Forecasts (ECMWF) analyses. The synoptic study shows that the upper-level front moved without significant change over the radar during the observation period, from 0000 UTC 14 November 1987 to 0000 UTC 15 November 1987. This allows radar data height–time cross sections to be interpreted as representing the corresponding spatial data distributions. A radar technique of stable airmass detection using the measurement of the aspect ratio, that is, the vertical to oblique power ratio, and the turbulence, that is, the structure constant of the refractive index fluctuations C_N^2, is developed. This method is applied to the case study of the upper-level frontal passage, which allows the associated stable air masses above the radar site to be monitored when going from 9 km down to the lower troposphere in the 2–4-km altitude range. Mesoscale dynamical aspects of the upper-level frontal zone are described using time series of radar-derived vertical wind shear. The 0.3° slope of the upper-level front, evaluated from the radar data and a 20 m s^{-1} eastward propagation velocity of the large-scale baroclinic system, agrees well with the one derived from radiosounding data of the nearest synoptic stations. Along this slope, an enhancement of the turbulence and a maximum vertical wind shear of 20 m s^{-1} km^{-1} were found. At a larger scale (timescale of 6 h), the reliability of the VHF-ST radar measurements of the air vertical velocity in the vicinity of the frontal zone is supported by both a favorable cross comparison with the vertical velocity calculated from the ECMWF analyses and downward motions roughly deduced from the winds on the isentropic surfaces.

1. Introduction

The Mesoscale Frontal Dynamic Project (MFDP/FRONTS 87) focused on the dynamics of active cold fronts between England and France from October 1987 to January 1988 (Browning et al. 1986; Thorpe et al. 1987; Clough 1987). The experiment involved observational networks, such as sodars, radars [dual-Doppler and stratospheric–tropospheric (ST)], radiosondes, dropsondes, and aircraft, to obtain an improved understanding of the dynamics of cold fronts during intensive observation periods (IOP). The multiple fronts and rainbands observed during the first part of the IOP 2, 11–14 November 1987, have been studied by numerous authors: Thorpe and Clough (1991) discussed the mesoscale dynamics of cold fronts as described by dropsoundings, Sortais et al. (1993) documented the dynamical and diabatic processes involved in the coupling between low- and upper-level jet–front systems, Redelsperger and Lafore (1994) used a 2D nonhydrostatic cloud model to simulate the IOP2, and Fisher and Lalaurette (1995a,b) performed 2D hydrostatic simulations to investigate the occurrence of conditional symmetric instability. In the present study, data time series obtained by a very high frequency (VHF) ST, radar (i.e., a clear-air radar at VHF frequency allowing stratospheric and tropospheric wind and turbulence profiling) are used to describe the passage of an upper-level frontal zone embedded in the baroclinic westerlies on the west side of an upper-level trough during the second part of the IOP 2, 14 November 1987.

Observations of frontal passages using VHF-ST radars have already been reported in several papers (e.g., Röttger 1979; Larsen and Röttger 1985; Neiman and Shapiro 1989; Crochet et al. 1990b; May et al. 1991;

Corresponding author address: Dr. J.-L. Caccia, Laboratoire de Sondages Electromagnetiques de l'Environment Terrestre, Universite de Toulon et du Var, BP 132, 83957 La Garde Cedex, France.
E-mail: caccia@lseet.univ-tln.fr

Neiman et al. 1992). In those experimental studies, the wind and/or the vertical reflectivity fields were used to describe the mesoscale height–time structure of the frontal zone above the radar site. Since the radar vertical reflectivity depends both on the atmospheric static stability and on the isotropic turbulence (Gage and Balsley 1980; Röttger 1980), the height–time atmospheric regions of high static stability could be derived from radar vertical reflectivity enhancements provided that the isotropic turbulence is not preponderant. Using this method, Röttger (1979), Larsen and Röttger (1985), and May et al. (1991) have been able to detect stable air masses exchanged between the stratosphere and the troposphere and the associated tropopause breaks or folds. Gage and Green (1978) and Röttger and Liu (1978) were first to use the enhancement of the radar vertical reflectivity to determine the tropopause altitude. As an application, a successful systematic comparison between tropopause heights obtained from this enhancement and from radiosoundings was found during a 3-month period (Green and Gage 1980). On the other hand, in these works, stable air layers were impossible to detect in the low troposphere because of the presence of very strong turbulence that resulted in both significant temperature and humidity fluctuations.

It is the purpose of the present paper to propose a method for taking into account the isotropic turbulence contribution to the radar vertical reflectivity using the simultaneous knowledge of the echo power obtained from two oblique radar beams slanted at 15°, which is known to be dependent on the isotropic turbulence only (Hocking et al. 1990; Luce et al. 1996). The radar parameter used in this method is the aspect ratio, that is, the vertical to oblique echo power ratio, interpreted as an atmospheric static stability signature. In addition to this parameter, quantities derived from the radar data, like the isotropic turbulence intensity, C_N^2, as well as the vertical shear of the horizontal wind, are used to evaluate the capabilities of the radar to describe the tropopause break, the slope, and the turbulence associated with the upper-level frontal zone. As previously mentioned, compared with the other papers on the same topic, the main originality of this study is to use both the aspect ratio and the turbulence intensity, which allows a more complete description of the upper-level frontal zone above the radar site, especially when the associated stable air goes down into the low troposphere. From a geophysical viewpoint, another important aspect of the present paper is that the synoptic situation of our case study was so that the upper-level front moved without significant change over the radar during the observation period, allowing radar height–time cross sections to be interpreted as representing the corresponding spatial data distribution.

Section 2 describes the synoptic-scale aspects of the upper-level dynamics of the baroclinic wave using uninitialized European Centre for Medium-Range Weather Forecasts (ECMWF) analyses and routine upper-level radiosounding data from the European synoptic network. The slope of the upper-level frontal zone over the VHF-ST radar site is evaluated. Section 3 describes the experimental conditions including the characteristics of the VHF-ST radar used in this study. The horizontal wind and the vertical wind shear derived from the radar data are presented and discussed in section 4. Still in section 4, the method of detection of the stable air using the turbulence and aspect ratio radar measurements obtained from one vertical beam and two oblique beams at 15° from the zenith is described in detail. Those radar-derived quantities are used to analyze the mesoscale aspects of the upper-level frontal zone and to be compared with data obtained from ECMWF analyses. A discussion concerning the validity of the air vertical velocity obtained from both the VHF-ST radar and the ECMWF model is presented in section 5. A summary of the results and their implications are given in section 6.

2. Synoptic situation from ECMWF analyses

Data for this study are taken from the uninitialized analyses produced by the T106/L19 operational model of the ECMWF, interpolated to a 150-km grid on a Lambert conformal projection, centered at 45°N, 17°W and true at 30° and 60°N. The grid consists of 32 points in the x and y directions. Map scale factors are included in all the diagnoses derived here. Gridded datasets are prepared on 19 pressure levels from 1000 to 100 hPa with a vertical spacing of 50 hPa. Five ECMWF analyses obtained every 6 h, from 0000 UTC 14 November 1987, through 0000 UTC 15 November 1987, are used.

The synoptic evolution of the baroclinic wave in which is embedded the upper-level frontal zone is analyzed through depiction of the geopotential height on the dynamic tropopause (Fig. 1). Although height is not conserved on a potential vorticity (PV) surface, it is found to be useful in tracking the tropopause break and the associated upper-level frontal zone observed by the radar. We use the following PV expression in isobaric coordinates;

$$\mathrm{PV} = g(f\mathbf{k} + \boldsymbol{\nabla}^p \times \mathbf{V}_h)\boldsymbol{\nabla}^p\theta, \qquad (1)$$

where PV is the Ertel potential vorticity, g the gravitational acceleration, f the Coriolis parameter, $\mathbf{V}_h$ the horizontal wind vector, $\boldsymbol{\nabla}^p$ the quasi-horizontal vector gradient, and θ the potential temperature. Using (1), the dynamic tropopause is defined as the 2.0-PVU surface (Hoskins et al. 1985). As shown in Fig. 1, the upper-level wave is progressing southeastward across Europe with a zonal phase speed of about 20 m s^{-1}. On the west side of the upper-level trough, a meridionally oriented tropopause break lies in the sharp gradient of tropopause height between 8 and 10 km. It moves across Brittany (area of northwestern France surrounded by the Atlantic coasts on the south, west, and north) between 0600 and 1200 UTC 14 November 1987. Winds aloft (~300 hPa) at 1200 UTC 14 November (Fig. 2) feature

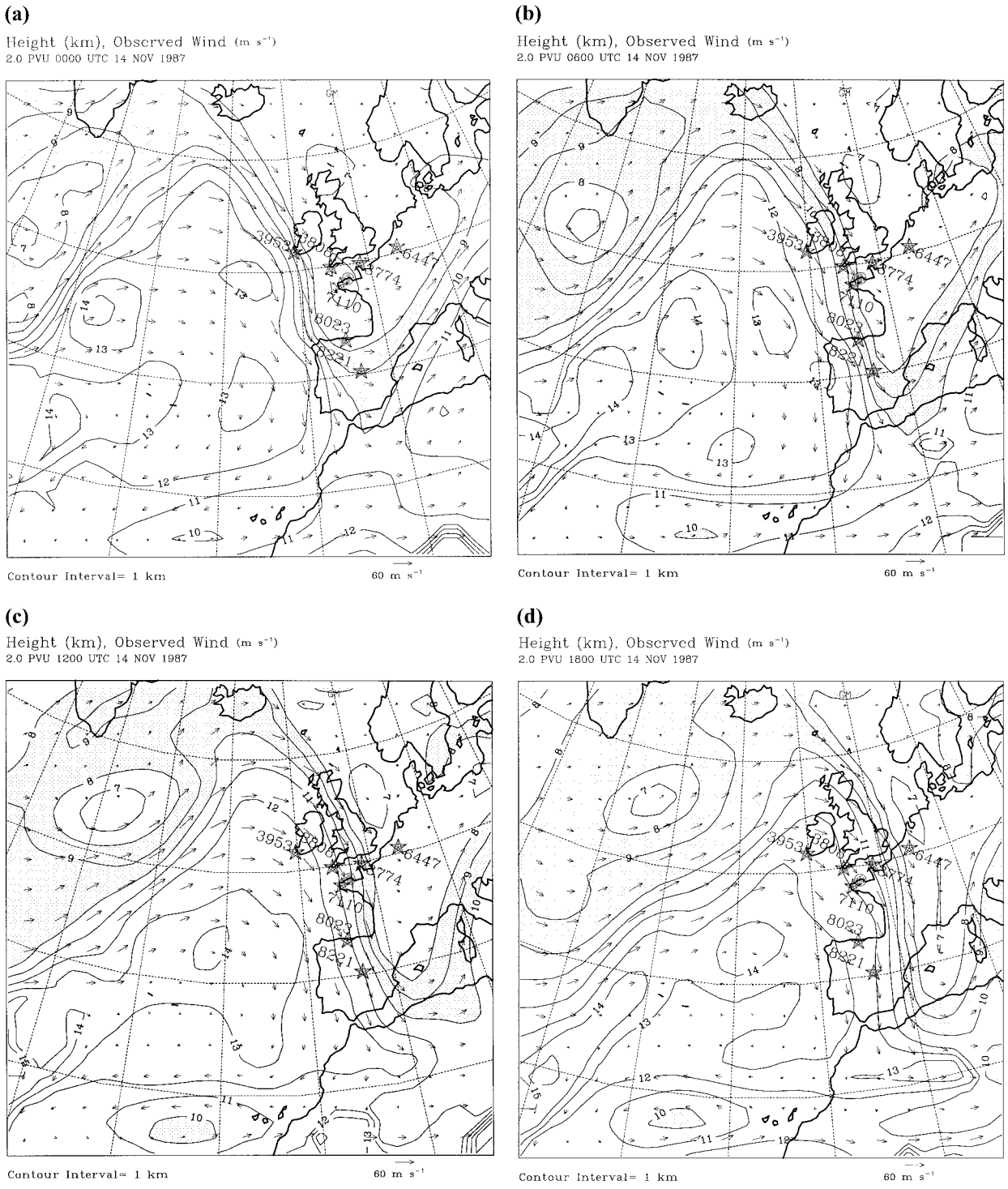

FIG. 1. Tropopause maps on the surface 2 PVU, 14 November 1987 at (a) 0000, (b) 0600, (c) 1200, and (d) 1800 UTC from the ECMWF analyses. Contours of tropopause height are in kilometers and tropopause winds in meters per second. The contour interval is 1 km and the shading corresponds to height between 8 and 10 km. The stars denote the positions of the radiosounding stations used, together with their numbers, whereas the hatched disk denotes the VHF radar site.

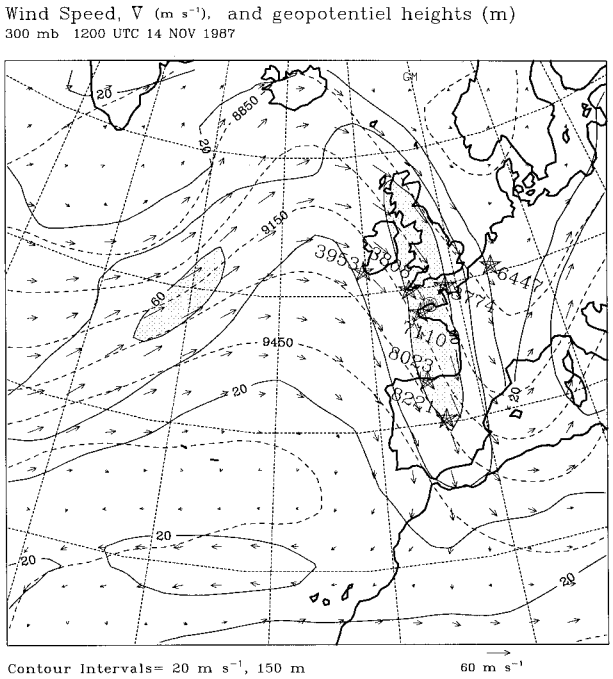

FIG. 2. The 300-hPa isotachs (solid lines, contour interval of 20 m s^{-1}, the shading corresponds to speeds in excess of 60 m s^{-1}), isohypses (dashed lines, contour interval is 150 m) and wind vectors at 1200 UTC 14 November 1987 from the ECMWF analyses. The stars denote the positions of the radiosounding stations used, together with their numbers, whereas the hatched disk denotes the VHF radar site.

a strong jet streak with speeds in excess of 60 m s^{-1}. According to the quasigeostrophic theory, the equatorward motion of the trough (see Fig. 1) agrees with the strongest winds being upstream from the trough (see Fig. 2).

Radiosounding data (1200 UTC 14 November 1987) at stations denoted by stars in Fig. 2 are analyzed to depict the upper-level frontal zone associated with the baroclinic wave. In Fig. 3, the radiosounding stations are aligned in the cross-front direction north of the VHF radar site and those used in Fig. 4 sample a cross section in the along-jet direction below the jet-core axis (see Fig. 2). Station 3953 (United Kingdom) stands on the anticyclonic shear side of the upper-level jet stream (tropopause above 200 hPa), and station 6647 (Netherlands) stands on the cyclonic shear side (tropopause just above 400 hPa). Station 3808 (United Kingdom) near the jet-core axis (see Fig. 2) exhibits the signature of the upper-level frontal zone just above 500 hPa. The cross-sectional analysis of potential temperature and along-front winds over the previous stations, that is, in the cross-front direction, is displayed in Fig. 5. The thermal stratification shows the slope of the tropopause and a well-defined upper-level frontal zone that descends from east to west in the cross-front direction. The along-front wind has a strong midtropospheric vertical shear below the jet core. All four radiosounding stations used in Fig. 4 show evidence of resembling characteristic features like the high tropopause slightly above 200 hPa and the upper-level frontal zone at 500 hPa. The cross-sectional analysis of potential temperature made with those four stations in the along-front direction (Fig. 6) shows evidence of a midtropospheric stable layer.

Of interest in this case study is to evaluate how strongly the upper-level frontal zone embedded in the baroclinic wave experiences changes when passing over the VHF radar in Brittany. In this case, the tropopause break line progresses eastward with a constant velocity and without large changes. Also, the tropopause height and the upper-level frontal zone altitude are quite the same in the along-jet direction. So we are assuming the applicability of the Taylor's hypothesis in order to do time to space conversion of radar data time series.

The slope of the upper-level frontal zone in this case is approximately 0.3° or equivalently 5.3 m km^{-1}. It is retrieved on the basis of the height of isentropic surfaces using radiosounding stations in the cross-jet direction. We use the 310-K isentropic surface, which is near the middle of the upper-level frontal zone (see Figs. 5 and 6 and arrows in Figs. 3b and 3c). Considering the 20 m s^{-1} zonal phase speed of the synoptic system, the height–time slope of the upper-level frontal zone in a vertical time series over the radar site is then close to -380 m h^{-1}, considering that the radar has sampled a transverse cross section of the upper-level jet.

3. Experimental conditions of the VHF-ST radar

The VHF-ST radar ''Provence'' is of the so-called Platteville radar type as those described by Gage and Balsley (1978) or Larsen and Röttger (1982). Its classical measurements are time evolution of the vertical profiles of the three wind components and of the atmospheric reflectivity observed in three directions (Crochet 1990). In summary, the wind velocity is estimated from the frequency corresponding to the mean Doppler shift obtained in the radar echo, whereas the reflectivity is estimated from the signal-to-noise ratio in the corresponding Doppler spectrum. During the MFDP/FRONTS 87 experiment, this radar was installed at Lannion, France (48.75°N, 3.43°E), with a frequency of 45 MHz, a peak power of 50 kW, an average power of 1 kW, and Doppler spectra calculated on 64 points. Experimental results already presented (Crochet et al. 1990a,b) have shown the reliability of measurements in mesoscale atmospheric dynamics. The vertical profiles of wind and reflectivity were obtained every 5 min 30 s, the acquisition time for each profile associated to one particular direction having been 1 min 50 s. The radar was sequentially switched among three different antennas of which one was pointed vertically upward and the other two were slanted at 15° to the vertical and had azimuthal orientations pointing toward the south and west. Here, half-hourly averaged data from 0000 UTC 14 November to 0000 UTC 15 November are used. A

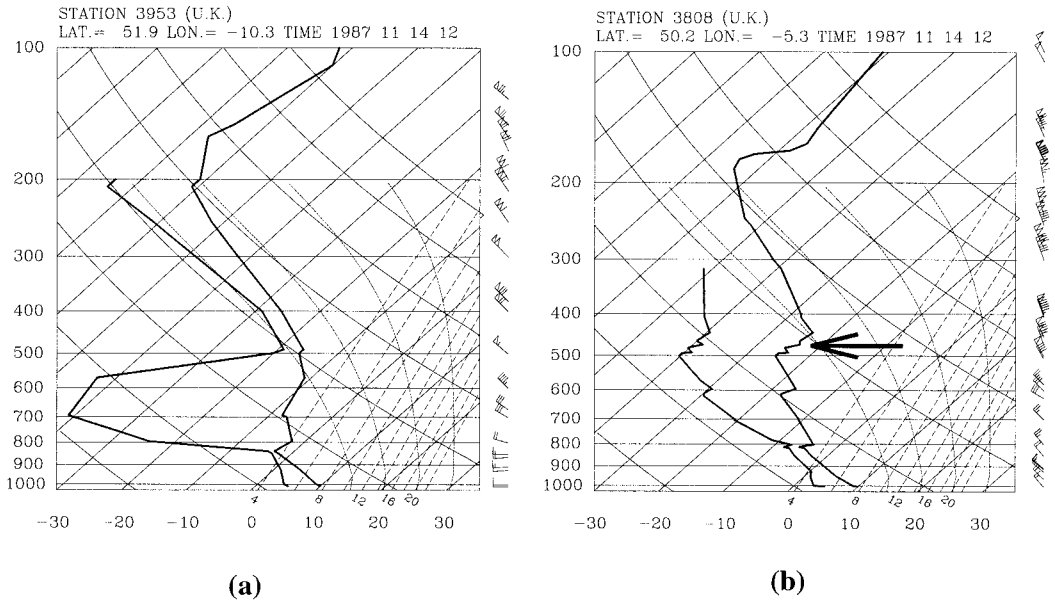

FIG. 3. Vertical soundings of synoptic stations in the cross-jet direction. (See the 3953, 3808, 3774, and 6447 stations of Figs. 1 and 2.) This set of stations is used to document the transverse cross section of the upper-level jet–front system just upstream of the VHF-ST radar. The two arrows, in (b) and (c), indicate the 310-K isentropic surface (at the middle of the upper-level frontal zone) at stations 3808 and 3774, respectively.

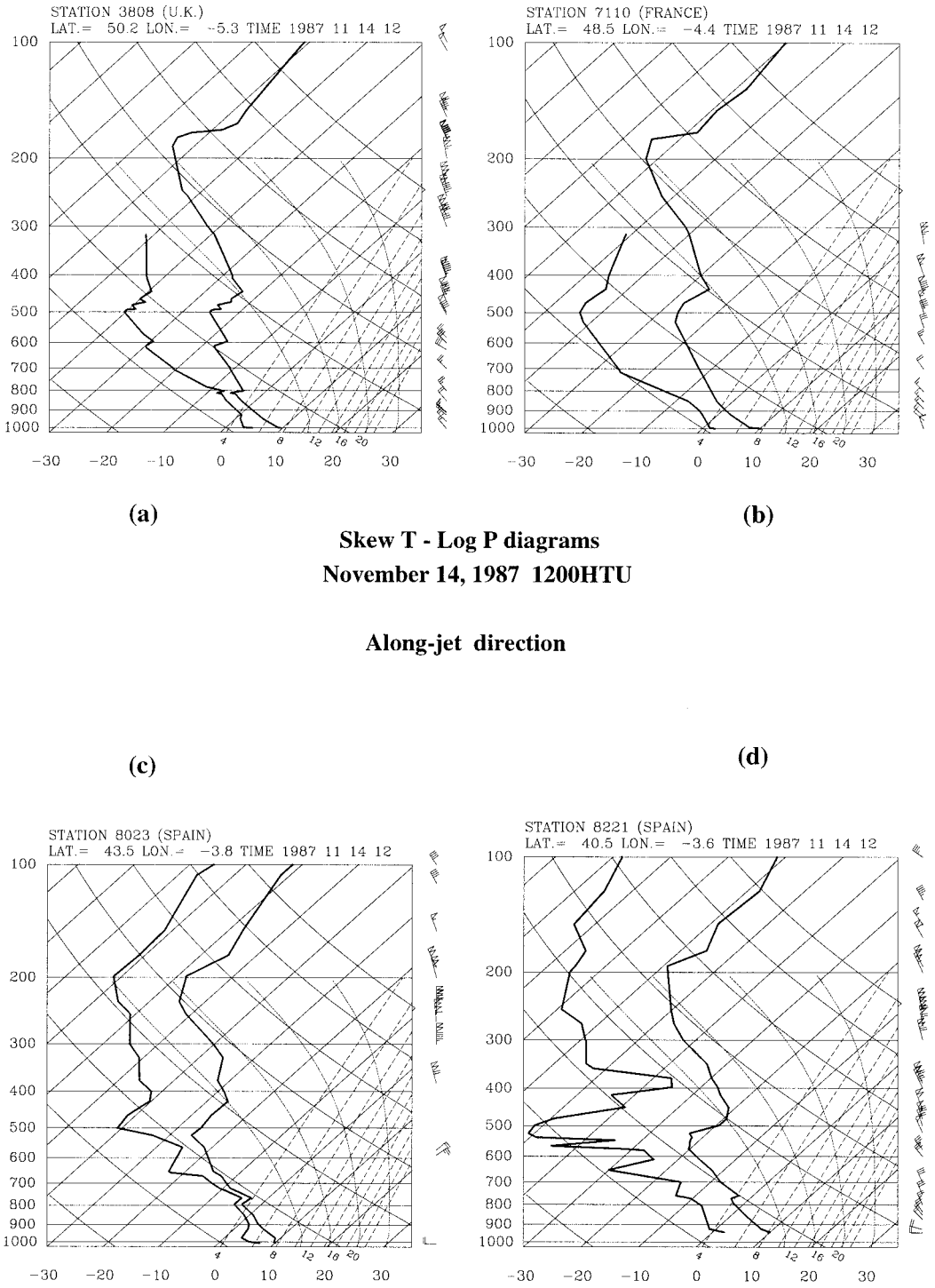

FIG. 4. Vertical soundings of synoptic stations in the along-front direction of the upper-level jet axis. (See the 3808, 7110, 8023, and 8221 stations of Figs. 1 and 2.) The northernmost station (a) is also used in Fig. 3 (b). The radiosounding station of Brest (b) is situated 85 km from the VHF radar location.

radar pulse and 30 gates of 4-μs length allowed us to investigate the atmosphere from 1200 up to 18 600 m with a vertical resolution and sampling step of 600 m. Nevertheless, only profiles from 1800 to 12 600 m, that is, for 19 successive altitudes, are used here to avoid any ambiguity in the data interpretation due to noise contamination and receiver saturation effects, respectively, at highest and lowest altitudes. Because of the

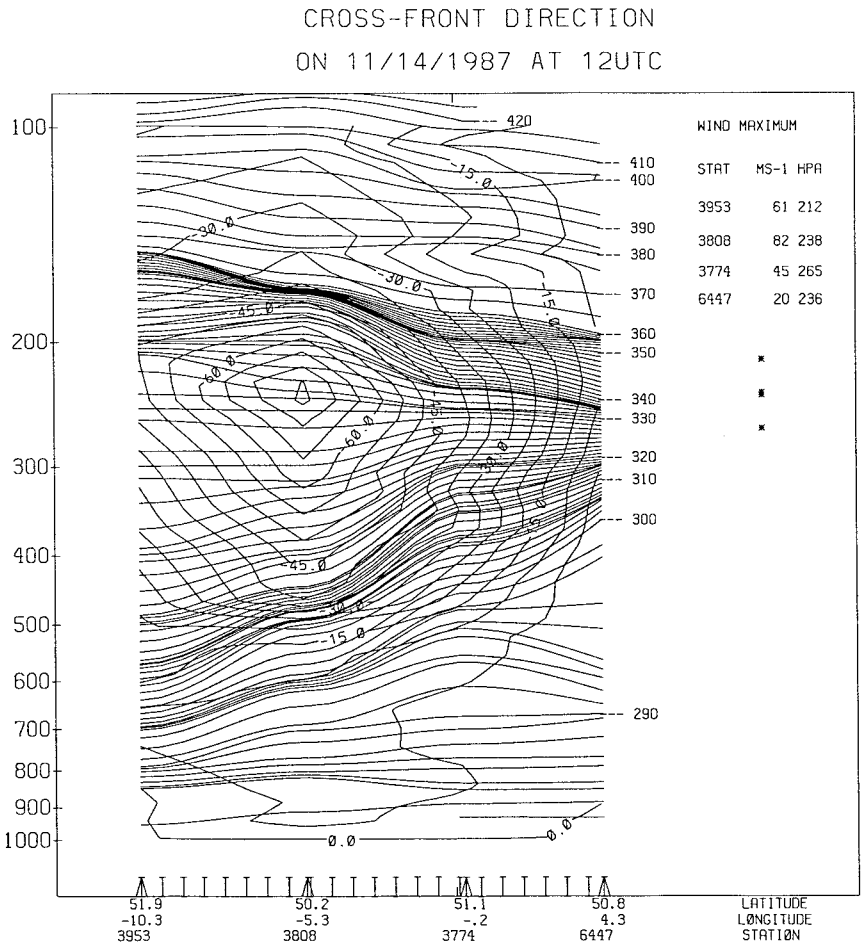

FIG. 5. Cross-sectional analysis of potential temperatures and along-front winds in the cross-front direction with stations 3953, 3808, 3774, and 6447. (See Figs. 1 and 2.) Distance between each station is approximately 400 km. Fields are interpolated using a cubic spline method.

off-zenith angle of 15°, the corresponding altitude range for the oblique beams is 1740–12 170 m, whereas the altitude resolution is 580 m. The tangential resolution is given by the radar beamwidth, here 5.5° at −3 dB, and ranged from 170 m, at 1800 m of radial distance, to 1210 m at 12 600 m. For the following, it is important to notice that the set of the three profiles sequentially obtained can be considered to be simultaneous since the 1-min 50-s delay is quasi-instantaneous according to both the timescales of the meteorological phenomenon studied and to the 30-min data averaging time.

4. Observation of upper-level features using ECMWF and VHF radar data

a. Horizontal wind and vertical wind shear

Several previous investigations (e.g., Ecklund et al. 1979; Fukao et al. 1982; Strauch et al. 1987) have established the capability of ST radars sufficiently well to provide reliable data on the horizontal wind velocity vector. The wind components are obtained from the radial velocities measured in three successive directions, that is, one vertical and two oblique directions, using the Doppler-shifted frequency in the corresponding received echo. The height–time cross section of the wind strength observed by the radar is shown in Fig. 7. Data are averaged with a 6-h moving window in order to be directly compared with the ECMWF analyses. Time series of vertical profiles over the VHF radar site obtained through spatial and temporal interpolation of the gridded ECMWF data are used to be compared to those obtained by the radar. Figure 8 shows the height–time cross section of the horizontal wind strength calculated from the ECMWF interpolated data. Winds in Figs. 7 and 8 are in good agreement except that at the level of maximum wind (i.e., between 1200 and 1800 UTC and around 10 km of altitude) the jet-core wind speed range of 65–75 m s^{-1} found by the ECMWF model is found to be 55–62 m s^{-1} by the radar. Although this difference could simply be attributable to the averaging–smoothing method applied to the radar data, or to possible overestimations made in the ECMWF analyses, it is also

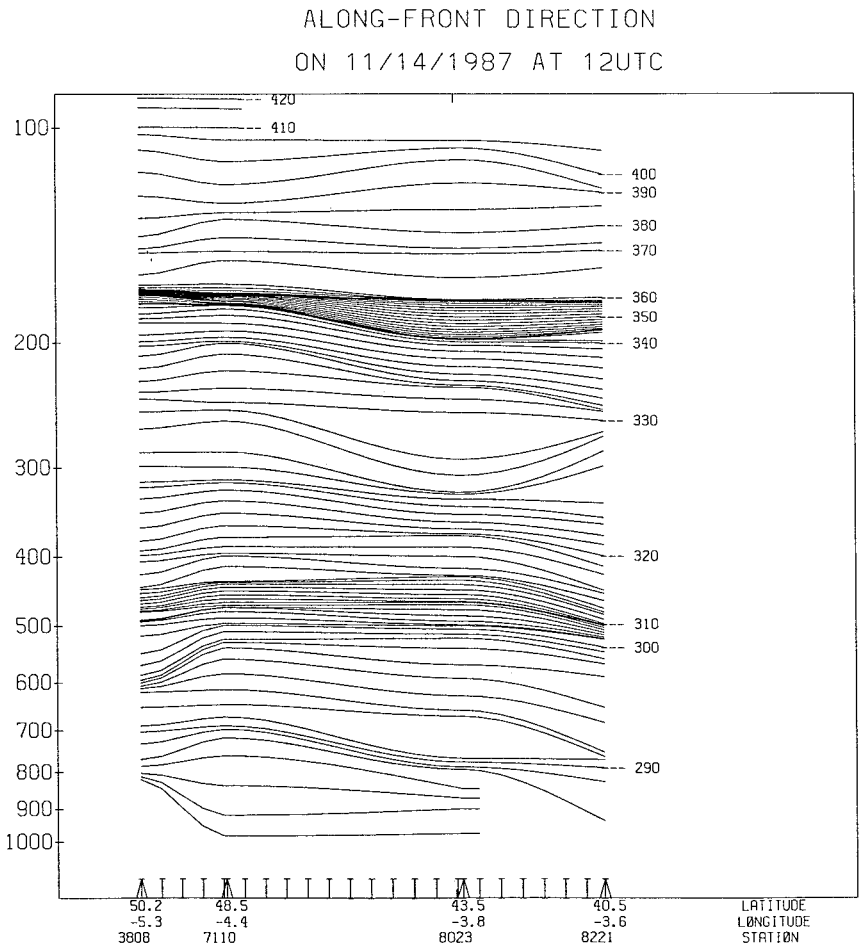

FIG. 6. Same as Fig. 5 but in the along-front direction with stations 3808, 7110, 8023, and 8221. Wind is not displayed in this along-jet cross section as it does not add other information than displayed in Fig. 4 due to the rather coarse horizontal resolution of the radiosounding stations.

consistent with VHF-ST radar measurement problems discussed by Yoe et al. (1994). They found that the horizontal wind maximum observed by a VHF-ST radar (the SOUSY-VHF radar, with oblique beams tilted at 7° and 10° from the zenith, in their case) at the height of a jet core may be underestimated by as much as 10 m s^{-1}. This bias is caused by the radar aspect sensitivity leading to an effective oblique-beam zenith angle smaller than the angle of the oblique-beam central axis and is compatible with the error possibly made in the radar measurements presented here. To deepen this discussion is not our purpose here; however, it is necessary to mention this possibility.

The dynamical mesoscale aspects of the upper-level front passage above the radar site can be investigated from the half-hourly averaged wind profiles (strength and direction) shown in Fig. 9. In a quasigeostrophic framework, it is possible to retrieve horizontal temperature gradients from the wind shear vector observations (Neiman and Shapiro 1989; Crochet et al. 1990a; May et al. 1991; Neiman et al. 1992). Thermal advection retrievals may then expand upon the diagnostics to investigate the forcing of vertical circulations embedded in upper-level jet streaks (Keyser and Shapiro 1986; Neiman and Shapiro 1989). Here, diagnostics of the magnitude of the total vertical wind shear vector are performed to put in a dynamical context the interpretation of the aspect ratio measurements made in the next section. The wind-shear magnitude $S(z, t)$ is calculated at an altitude z from the half-hourly averaged westward component vertical profile $U(z, t)$ obtained at a given time t, and the southward one $V(z, t)$ following (2) and (3):

$$S(z, t) = \left[\left(\frac{\Delta U(z, t)}{\Delta z}\right)^2 + \left(\frac{\Delta V(z, t)}{\Delta z}\right)^2\right]^{1/2}, \qquad (2)$$

with

$$\Delta U(z, t) = U\left(z + \frac{\Delta z}{2}, t\right) - U\left(z - \frac{\Delta z}{2}, t\right)$$

and

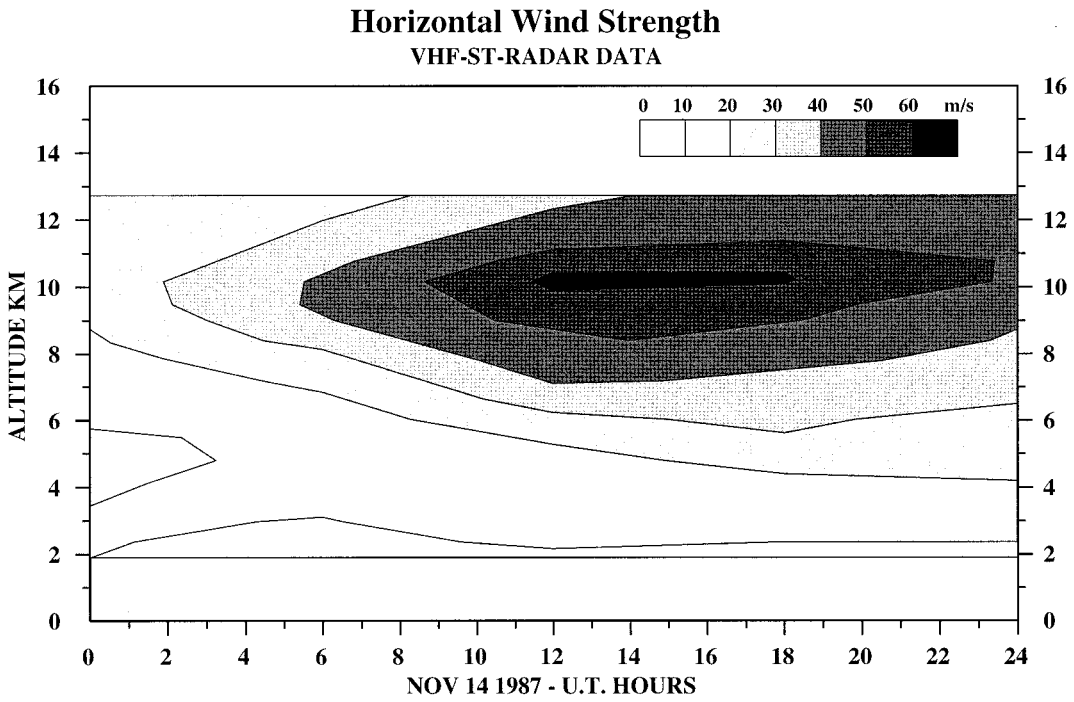

FIG. 7. Height–time cross section of the horizontal wind strength measured by the VHF-ST radar between 0000 UTC 14 November and 0000 UTC 15 November. The data are 6-h moving averaged, thus smoothed compared to the 5-min 30-s initial time resolution, but directly comparable to the ECMWF data shown in Fig. 8. The shadings used in the representation are indicated below the top axis.

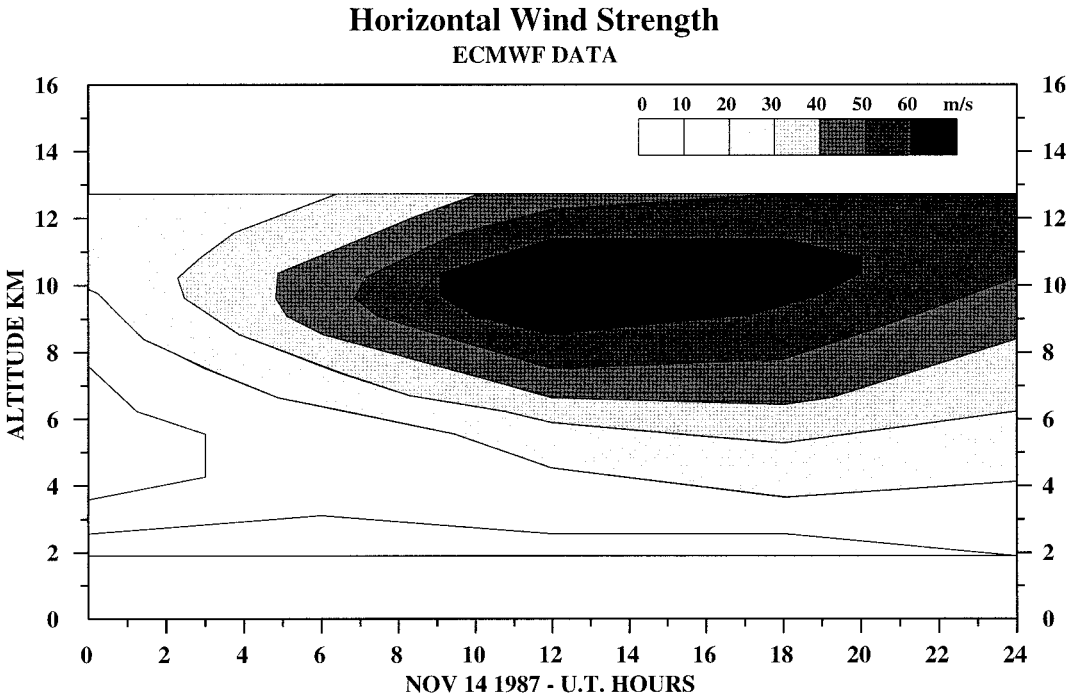

FIG. 8. Height–time cross section of the horizontal wind strength above the VHF-ST radar site vertically and temporally interpolated from ECMWF analysis data to be in the same height–time representation as the radar data shown in Fig. 7. The shadings are the same as in Fig. 7.

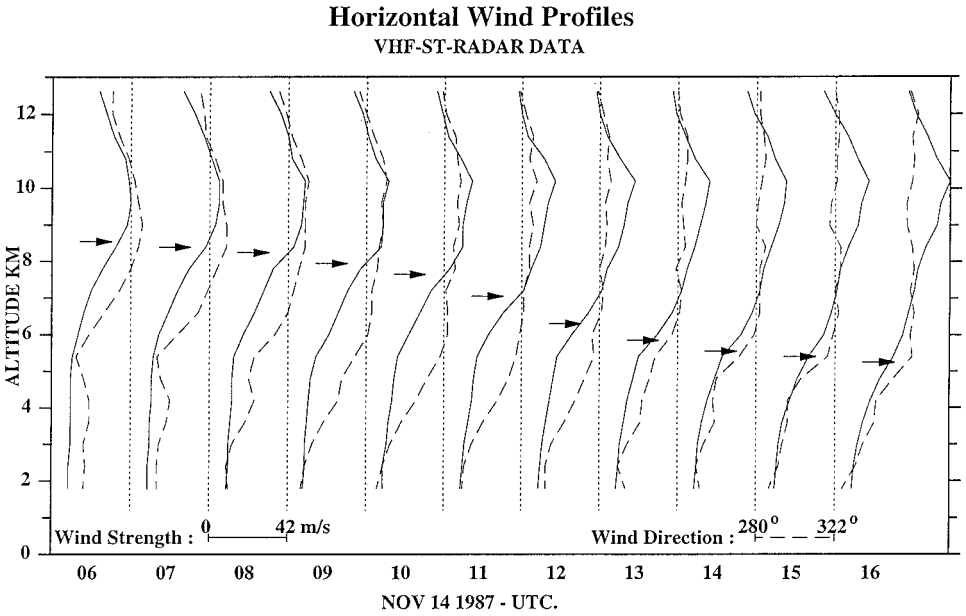

FIG. 9. Half-hourly averaged wind profiles obtained every hour by the VHF-ST radar. The solid and dashed lines refer to the wind strength and direction, respectively. For each profile, the vertical dotted line on the left indicates the corresponding y axis, a strength of 0 m s^{-1}, and a direction of 280° (westerly wind), whereas that on the right indicates a strength of 42 m s^{-1} and a direction of 322° (northwesterly wind). The arrows show the altitudes of maximum wind shear.

$$\Delta V(z, t) = V\left(z + \frac{\Delta z}{2}, t\right) - V\left(z - \frac{\Delta z}{2}, t\right), \quad (3)$$

and where Δz is the vertical resolution of 600 m of the radar profiles. The levels for which $S(z, t)$ is maximum are shown by the arrows in Fig. 9. At those levels, it is noticeable that the wind shear was also due to direction vertical variations. Locations in the height–time diagram where $S(z, t) > 10$ m s^{-1} km^{-1} are bounded by the dashed isocontours in Fig. 12, whereas the encapsulated thick solid line follows the maximum-value crest line, which reached 20 m s^{-1} km^{-1}, at 8100 m of altitude and at 0800 UTC. The wind shear value, averaged along this line was found to be 18 m s^{-1} km^{-1}, in magnitude, and 342°, that is, quasi-southward, in direction. In a quasigeostrophic framework, the direction of the wind shear vector is expected to give the approximate frontal orientation (Neiman et al. 1992). A good agreement is found here since the ECMWF analyses have shown a north–south orientation for the frontal surface. That solid line is also reported in Figs. 10, 11, and 16 to make our discussion easier. Presumably the underestimation of winds at the jet-core level smooths the retrieved height–time series of vertical wind shear magnitudes shown in those figures. Nevertheless, Fig. 12 clearly indicates two regions of maximum vertical wind-shear magnitude, the first one surrounds the jet core at the tropopause level and the second one, which is also the stronger, slants down into the troposphere below the jet core.

b. C_N^2 and aspect ratio measurement

It has been shown (e.g., Tsuda et al. 1986; Hocking et al. 1990; Luce et al. 1995) that the radar echo power obtained with an antenna tilted at more than 10° from the zenith is mainly due to isotropic turbulence. The same behavior can be assumed here since the two oblique beams used in our study have zenith angles of 15°. The amount of isotropic turbulence given by the C_N^2, that is, the refractive index fluctuation structure constant, is obtained by the classical radar equation (e.g., Röttger 1980) applied to the oblique echo power.

Gage and Green (1978) and Röttger and Liu (1978) evidenced that VHF echoes backscattered from overhead are much stronger than from an oblique direction. An explanation for this enhancement can be found in the papers by Gage and Balsley (1980) and Röttger (1980) where it is proposed that the vertical echo is caused by both isotropic turbulence backscattering and specular reflection due to the potential refractivity gradient. This gradient, which can be distributed within a radar cell in thin superimposed layers or sheets (Dalaudier et al. 1994; Luce et al. 1995) is proportional to the mean atmospheric static stability, that is, the square value of the Brunt–Väisälä (BV) pulsation, in the corresponding radar cell. The radar vertical reflectivity is thus suitable for stable airmass detection provided that the isotropic turbulence effect can be eliminated. To solve this problem, the calculation of the aspect ratio A_R, that is, the vertical-to-oblique echo power ratio, or equiva-

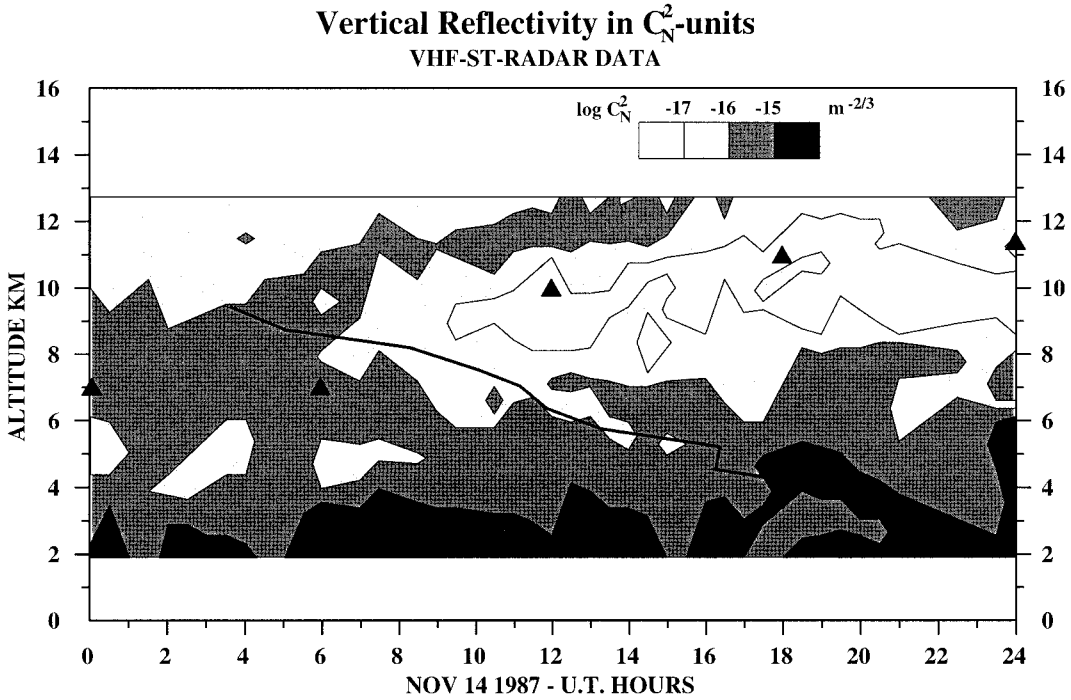

FIG. 10. Height–time cross section, from half-hourly averaged radar data, of the vertical-beam radar reflectivity measured in C_N^2 units ($m^{-2/3}$) and obtained between 0000 UTC 14 November and 0000 UTC 15 November. The shadings are labeled in log scale below the top axis. The maximum wind shear crest line (thick, solid line) is also indicated in Figs. 11, 12, and 16. The black triangles refer to the tropopause altitude obtained by the ECMWF analyses.

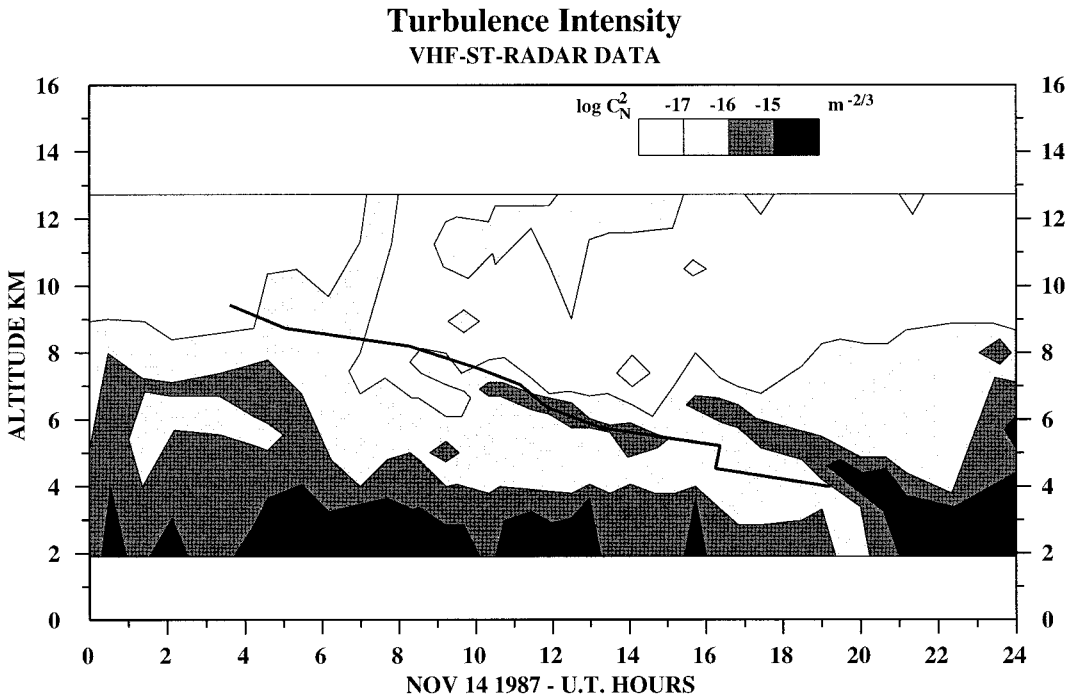

FIG. 11. Height–time cross section, from half-hourly averaged radar data, of the turbulence intensity, that is, the C_N^2 between 0000 UTC 14 November and 0000 UTC 15 November. The height–time cross sections obtained from both the eastward and the southward radar beam are averaged to obtain the figure presented here. The shadings are labeled in log scale below the top axis. The maximum wind shear crest line (thick, solid line) is also indicated in Figs. 10, 12, and 16 and coincides well between 1000 and 1500 UTC, with a layer of enhanced turbulence.

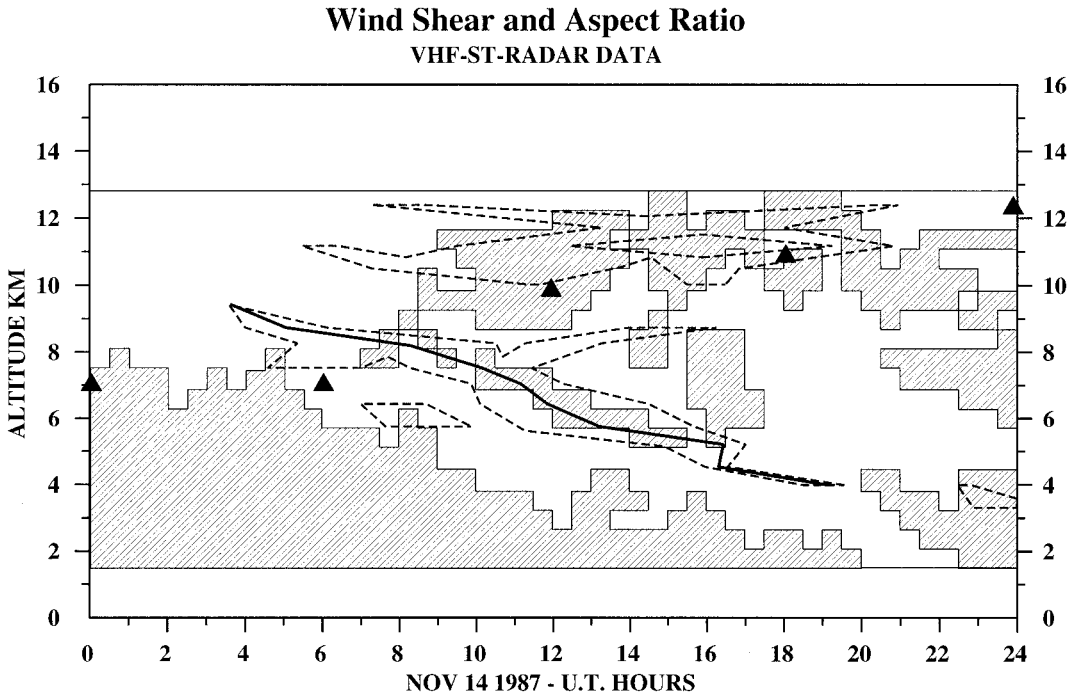

FIG. 12. Height–time cross section, from half-hourly averaged radar data, of vertical wind shear and aspect ratio from 0000 UTC 14 November to 0000 UTC 15 November. (See the text for detailed explanations about the aspect ratio calculation.) The wind shear values greater than 10 m s^{-1} km^{-1} correspond to the areas within the dashed-line contours. The upper and lower contours refer to wind shears due to, respectively, the jet-core passage and the upper-level frontal zone passage. The thick, solid line indicates the maximum value crest line and is also shown in Figs. 10, 11, and 16. The hatched parts correspond to aspect ratios smaller than 3, and the white parts to those greater than 3. The black triangles refer to the tropopause altitude obtained by the ECMWF analyses.

lently, the vertical-to-oblique beam C_N^2 value ratio, is particularly appropriate when using beams tilted at 15° as in our case. Clearly, at a given time and for a given radial distance, the A_R value quantifies the weight of the stability compared to that of the turbulence. For A_R values close to 1, the corresponding air mass essentially contains isotropic turbulence, whereas A_R values much higher than 1 refer to stable air.

The values of the vertical profiles of C_N^2 derived from the vertical beam and used for the A_R calculation were actually linearly interpolated so that the altitudes used for the three beams were the same. It is nevertheless noticeable that, except for this interpolation technique applying only to the data obtained from the vertical beam and not seriously affecting the calculation in the low troposphere, the processing was the same for the three radar beams.

Figures 10 and 11 show the height–time cross sections of the C_N^2 values obtained from the vertical and the oblique beams, respectively. The values of Fig. 10 are actually the radar vertical reflectivity expressed in C_N^2 units ($m^{-2/3}$), whereas those of Fig. 11 correspond to the amount of isotropic turbulence averaged for both of the oblique beams. As expected, the values from the vertical direction are found to be stronger than those from the oblique directions. The classical mean behavior of isotropic turbulence profile decreasing from the ground to the low stratosphere is clearly observed in Fig. 11. This same figure also reveals the presence of strong turbulence along the crest line of maximum wind shear magnitude. The enhancement of the vertical echo power due to stable stratospheric air masses is clearly visible after 0600 UTC in Fig. 10 and coincides well with the tropopause altitude calculated from the ECMWF analyses (see the black triangles). On the other hand, before 0600 UTC, this tropopause signature is masked by the presence of significant turbulence up to 8 km, that is, above the tropopause altitude. Furthermore, during the whole period studied, no stable air masses are clearly detected below 8 km. This illustrates the classical problem of VHF radar detection of the stable layer down to the low troposphere by only using the vertical reflectivity.

The height–time cross section of half-hourly averaged A_R values, calculated from the data of Figs. 10 and 11, is shown in Fig. 12 for the whole period studied. The hatched part indicates the height–time atmospheric regions where A_R is lower than 3 whereas the white one corresponds to A_R greater than 3. The C_N^2 ratios of the two oblique beams were also computed for the whole period studied and between 1800 and 6000 m, that is, for C_N^2 values systematically higher than 10^{-17} $m^{-2/3}$. Of

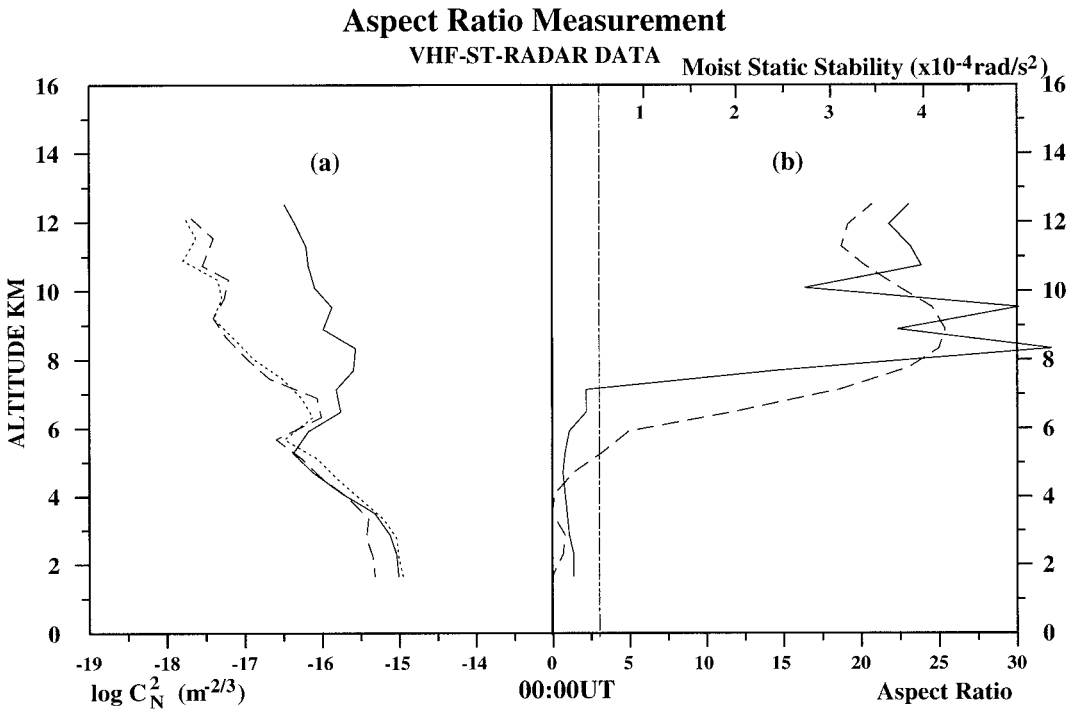

FIG. 13. (a) Vertical C_N^2 profiles, or profiles of isotropic turbulence in log scale, obtained from eastward (dotted line) and from southward (dashed line) radar beam measurements, at 0000 UTC 14 November 1987. The solid curve shows the vertical profile of the radar vertical reflectivity in C_N^2 units ($m^{-2/3}$) and in log scale. When the vertical reflectivity is significantly greater than the isotropic turbulence, the air is highly stable. (b) Vertical profiles of the aspect ratio (solid curve) calculated from the three curves of (a). (See the text for more details.) The bottom axis indicates the dimensionless aspect ratio values and the vertical dotted–dashed line corresponds to the value 3 beyond which the air is considered to be more stable than turbulent. The dashed–dotted curves, respectively, show the vertical profiles of the moist and dry static stability calculated from ECMWF analyses. This quantity is expressed as the square value of the corresponding Brunt–Väisälä pulsation. The values are indicated on the top axis.

the 392 calculated ratios, 96% were found in the ⅓–3 range (83% between ½ and 2). Since the calculation was made from oblique-beam measurements, the value of 3 can be seen as the largest A_R values obtainable in the case of isotropic turbulence scattering. This is the reason why the $A_R > 3$ criterion is used for stable air detection. In addition, a value of 1.17 was found by averaging the 392 C_N^2 ratios. This shows that a bias exists between the two oblique-power measurements but is very low, that is, 0.7 dB.

Figures 13, 14, and 15 are shown to illustrate our A_R calculation method. Figures 13a, 14a, and 15a show the vertical profiles of C_N^2 obtained from the two oblique measurements at 0000 UTC 14 November, 1200 UTC 14 November, and 0000 UTC 15 November, respectively. In each of these figures, the measurements obtained from the eastward and the southward beams are indicated by the dotted and dashed lines, respectively. The corresponding vertical reflectivity, calculated in C_N^2 units, is shown in the same figures by the solid lines. Then, the A_R profiles, shown by the solid lines of Figs. 13b, 14b, and 15b, are obtained by dividing the corresponding vertical reflectivity profile by the average of the two corresponding oblique-beam C_N^2 profiles.

c. *Moist static stability calculation from the ECMWF analyses*

As for the horizontal wind shown in Fig. 8, time series of vertical profiles of the moist static stability over the VHF radar site obtained through spatial and temporal interpolation of the gridded ECMWF data are used to be compared to the A_R values obtained by the radar. The moist static stability used to plot Fig. 16 and the dashed curves of Figs. 13b, 14b, and 15b is the square value of the BV pulsation and is derived as follows:

$$N^2 = \frac{g}{\theta_e}\frac{\partial \theta_e}{\partial z}, \tag{4}$$

where θ_e is the equivalent potential temperature and z is the altitude. The use of the moist static stability and its associated BV pulsation is appropriate in the lower troposphere when the air is saturated. During the period studied, a height of precipitation of 6 mm was recorded at Lannion (information provided by the French National Meteorology), that is, in the area where the radar was installed. At higher levels and for weaker water vapor mixing ratios, the moist and dry static stabilities are very similar. In order to show this behavior, vertical

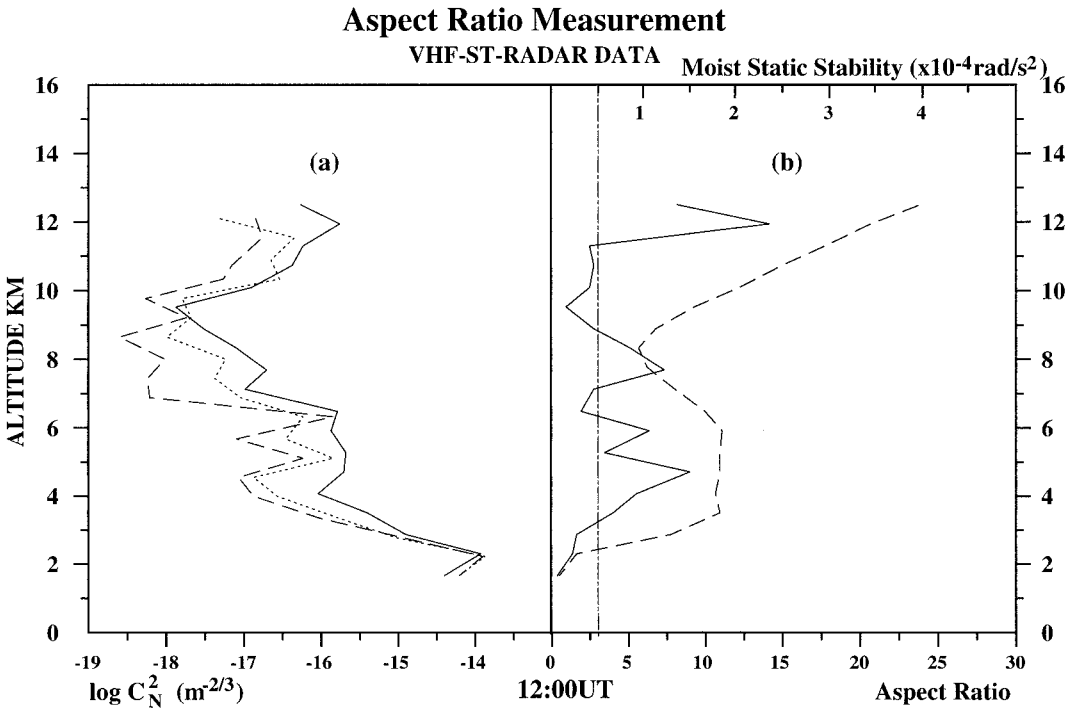

FIG. 14. Same as Fig. 13 but for 1200 UTC 14 November.

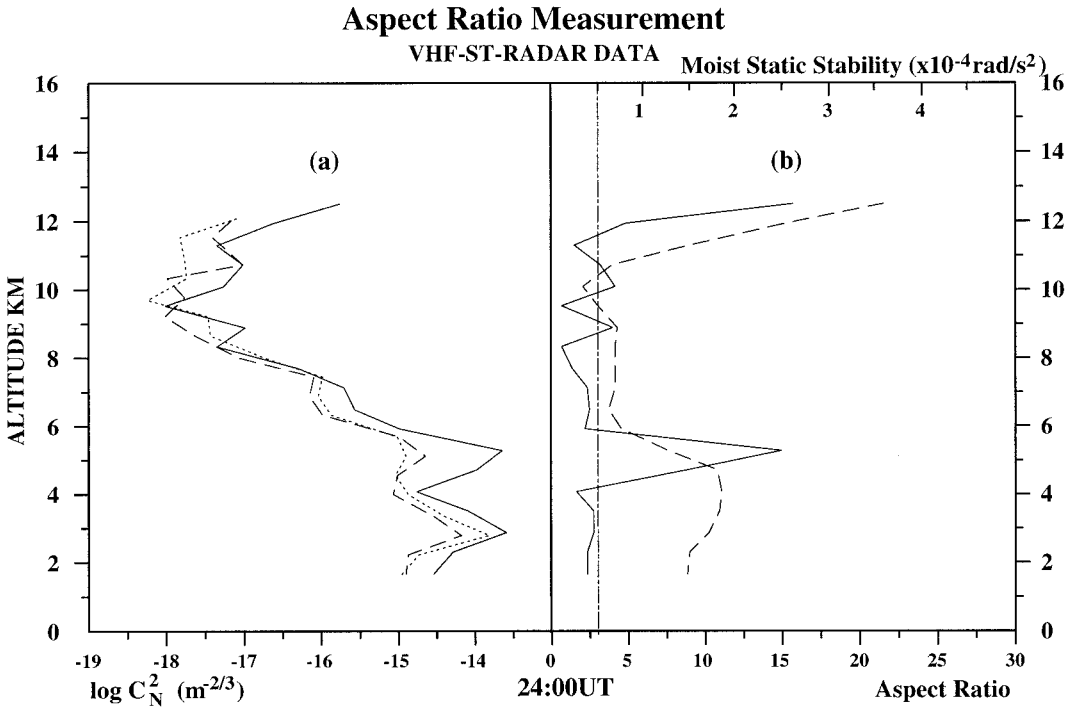

FIG. 15. Same as Fig. 13 but for 0000 UTC 15 November.

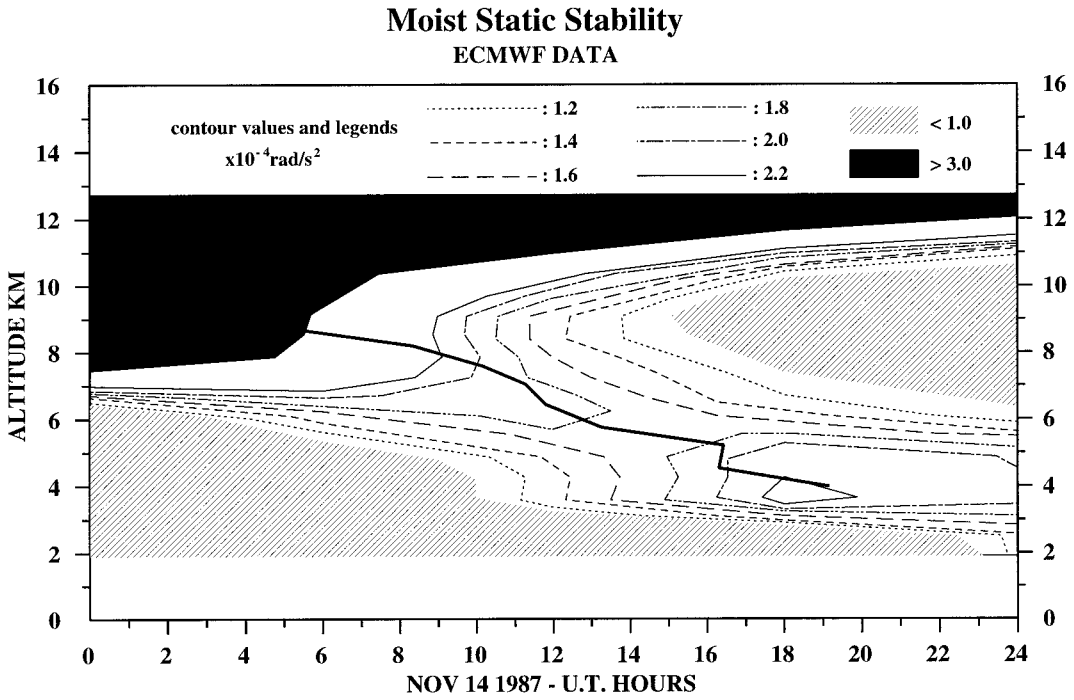

FIG. 16. Height–time cross section of moist static stability from spatially and temporally interpolated ECMWF gridded data from 0000 UTC 14 November 1987 to 0000 UTC 15 November 1987. Contour intervals and shadings are labeled below the top axis. The thick, solid line denotes the crest line of the maximum vertical wind shear observed by the VHF radar. This crest line is also depicted in Figs. 10–12.

profiles of dry static stability are also plotted in Figs. 13b, 14b, and 15b (dotted curves). For these profiles, the BV pulsation values are calculated by replacing θ_e with θ, that is, the potential temperature in (4). In Fig. 16, evidence of a tropopause-break occurence at 9-km height and between 0600 and 1200 UTC is shown by the vertical slope of the highest contours of the moist static stability. A clear signature of the upper-level frontal zone passage is shown by the downward penetration of the stable air from the tropopause level at 0600 UTC down to 4 km at 1800 UTC. At 1200 UTC, the altitude of the upper-level frontal zone as seen with the ECMWF analyses is close to 6.5 km, which is in good agreement with the one observed at the nearest radiosounding station, 7110 (48.5°N, 4.4°W) over Brest (Fig. 4).

d. Data comparison and discussion

The first data comparison concerns the moist static stability calculated from the ECMWF analyses [(4), Fig. 16], and both the VHF radar reflectivity (Fig. 10) and the radar aspect ratio (Fig. 12). A rather good general agreement is found between the high static stability area and the area of A_R values greater than 3 (white part of Fig. 12). This result shows that an aspect ratio greater than 3 is a good tracer for stable air detection most of the time. Nevertheless, some areas of disagreement are found between Fig. 12 and 16. The one in the vicinity of the frontal zone collocates a relatively strong turbulent layer. A comparison between Figs. 11 and 12 shows that this strong turbulence actually collocates the region of relatively low A_R values encapsulated in the dashed contour surrounding the crest line of maximum wind shear magnitude, which corresponds to the frontal zone (e.g., May et al. 1991). Therefore, those low A_R values can be interpreted as more due to a strong turbulent layer than to weakly stable air. Similarly, the area of weak A_R values in the upper-central part of Fig. 12 is probably due to the turbulence enhancement obtained at the same location in Fig. 11. The same explanation can be used for the lower-right area of weak A_R values of Fig. 12, which corresponds to the lower-right area of strong turbulence of Fig. 11. The others, irregularly distributed after 1400 UTC and above the frontal zone, are explainable by a too-strong A_R estimation noise due to weak stability and turbulence. This is probably the reason why the vertical reflectivity shown in Fig. 10 and obtained after 0600 UTC is more suitable than A_R for the tropopause height estimation (see the three higher black triangles of Figs. 10 and 12). On the other hand, when the tropopause altitude is lower than 8 km, the A_R method gives better results (see the two lower black triangles of Figs. 10 and 12). Also, the time evolution of the troposphere thickness before and below the frontal zone passage and obtained from the lower hatched part of Fig. 12 is in very good agreement with that obtained in Fig. 16 from ECMWF analyses. Furthermore, three vertical profiles of the ECMWF moist static

stability are superimposed, as a dashed line, to the corresponding A_R solid-line profiles in Figs. 13b, 14b, and 15b. In these three cases, although the compared quantities are not homogeneous, a rather good agreement is obtained concerning their vertical variations. It is noticeable that, in our case study, the use of the dry static stability (dotted curves of Figs. 13b, 14b, and 15b), instead of the moist one, would not have significantly influenced the result of the comparison. In summary, although a too-strong A_R estimation noise and/or the presence of strong turbulent layers are responsible for some disagreements, $A_R > 3$ is a rather good criterion for stable air detection, mainly below 8-km height.

The maximum value crest line of vertical wind shear fits remarkably well with the tropospheric altitudes of the highest moist static stabilities derived from the ECMWF analyses (see Fig. 16). Furthermore, the slope of this radar-derived crest line is about -360 m h^{-1}, which is very close from the slope of -380 m h^{-1} of the upper-level frontal zone previously derived from radiosounding stations. As already mentioned, such an agreement was already found by May et al. (1991), for instance.

The strong turbulent layer detected along this maximum wind shear region (see Fig. 11), thus along the upper-level frontal zone, coincides well with a region of relatively high static stability. A simple calculation of the Richardson number, that is, the ratio of the static stability to the square value of the wind shear, leads to a mean value of 0.5 between 1200 and 1400 UTC along the maximum wind shear crest line. Such a positive and low value is classically considered to be consistent with a well-developed isotropic turbulence (e.g., Tennekes and Lumley 1972). It could thus be expected here that a turbulent layer along the frontal zone was detected by the VHF ST radar. Regions of clear-air turbulence are associated with large potential vorticity changes (Gidel and Shapiro 1979), therefore VHF-ST radar turbulence measurements may be worthwhile to use to investigate such a process.

5. Discussion on vertical velocity data

Favorable comparisons between synoptic-scale vertical velocities indirectly calculated and measured by a VHF-ST radar were already obtained by Nastrom et al. (1994). They used 6-h means of data from the Flatland VHF radar located in the very flat terrain of central Illinois (Green et al. 1988) in order to be far from mesoscale orographic influences that contaminate the synoptic-scale data comparison. Such effects were already evidenced by Nastrom et al. (1985) and Larsen et al. (1988), for instance. The purpose of this section is simply to present further results of comparison between numerical model and VHF-radar vertical velocity data in the framework of an upper-level front passage. Although such an atmospheric process is typically mesoscale, 6-h means of radar data are used to be directly compared with the 6-h ECMWF-model analyses.

In our case study, the kinematic calculation of the vertical motion from ECMWF horizontal velocities follows the O'Brien method (O'Brien 1970). From the equation of continuity we compute the vertically integrated divergence in order to obtain a first guess at the vertical velocity field. A linear correction is then applied to the divergence, and the vertical velocity is adjusted so that it vanishes at 1000 and 100 hPa. As previously, the data are vertically interpolated and resampled with the vertical resolution (600 m) of the VHF radar in order to be cross compared. The results are displayed in Fig. 17.

The VHF radar measurement of the vertical velocity is very controversial when the backscattering and/or reflecting layers above the radar are off horizontally tilted (e.g., Larsen and Röttger 1991; Larsen et al. 1991; van Baelen et al. 1991). Roughly, the more tilted the layer and the stronger the horizontal wind, the more significant the error made on the vertical velocity estimation. The vertical velocity data directly obtained from the vertically oriented antenna of the VHF radar, and 6-h averaged for comparison with ECMWF data, are shown in Fig. 18.

Yoe and Rüster (1992) have shown that the bias in the radar vertical velocity could be very significant at the jet stream altitude, due to a horizontal anisotropy of the backscattering layer and to strong horizontal wind velocities, here more than 60 m s^{-1}. This can explain the disagreement obtained between Figs. 17 and 18 above 9 km, that is, in the jet-core altitude range.

Another disagreement is found below 4-km altitude. A possible explanation comes from the fact that the radar site was in the lee of cliffs of 50–80-m height located along the northwestern Brittany coast. The lee waves induced at low altitudes are subgrid-scale effects that are not taken into account in the ECMWF T106 operational model used here. These lee waves, to which the vertical velocity measurement by VHF-ST radar is sensible, should be the main cause of disagreement between Figs. 17 and 18 below 4-km altitude. This was illustrated by a recent work (Lott 1995) in which its was shown that a subgrid parameterization of the orography (which is not included in the ECMWFT106 model) is necessary to minimize the model underestimations of the effect of local orography.

Especially interesting for our purpose is that a good agreement between Figs. 17 and 18 is found nearby the upper-level frontal zone passage, that is, between 0500 and 1900 UTC and between 4- and 9-km altitude. In this time–height range, the slope of the upper-level frontal zone is approximately 0.3° (see section 2). Such a low value, compared to a radar beam half-width of 2.75°, associated with the fact that the measurements are not made in the vicinity of the jet core, where the wind is very strong, should not lead to a significant bias in the vertical velocity estimation. This favorable cross

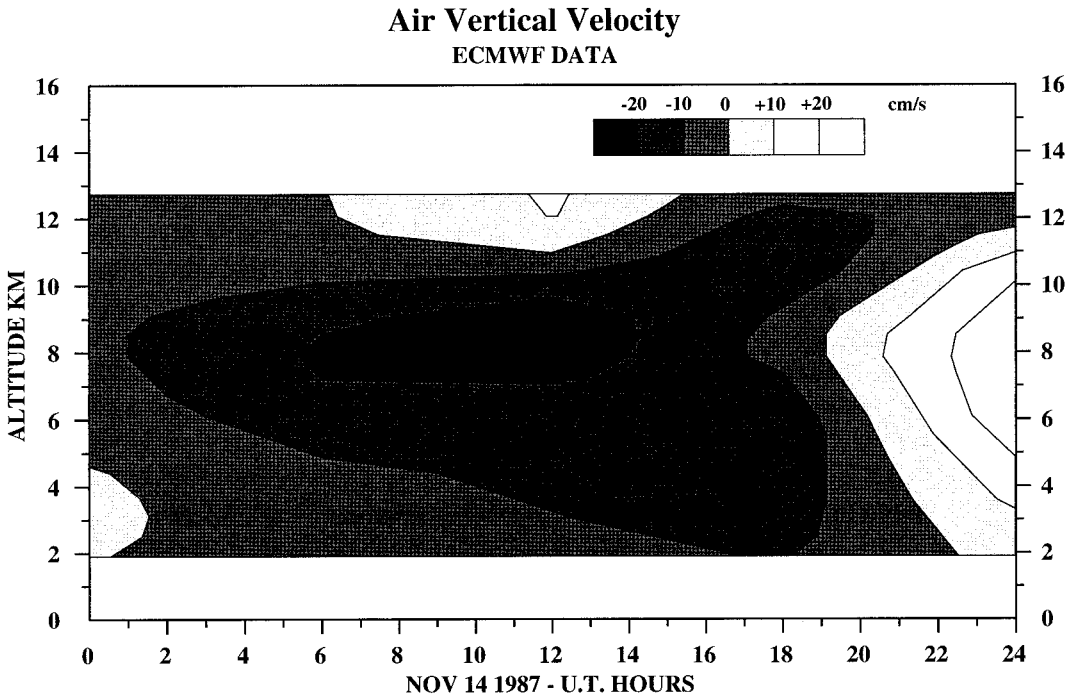

FIG. 17. Height–time cross section of kinematic vertical velocity from spatially and temporally interpolated ECMWF-gridded data from 0000 UTC 14 November 1987 to 0000 UTC 15 November 1987. The contour interval is 10 cm s^{-1} and the shadings are as the upper caption of the figure.

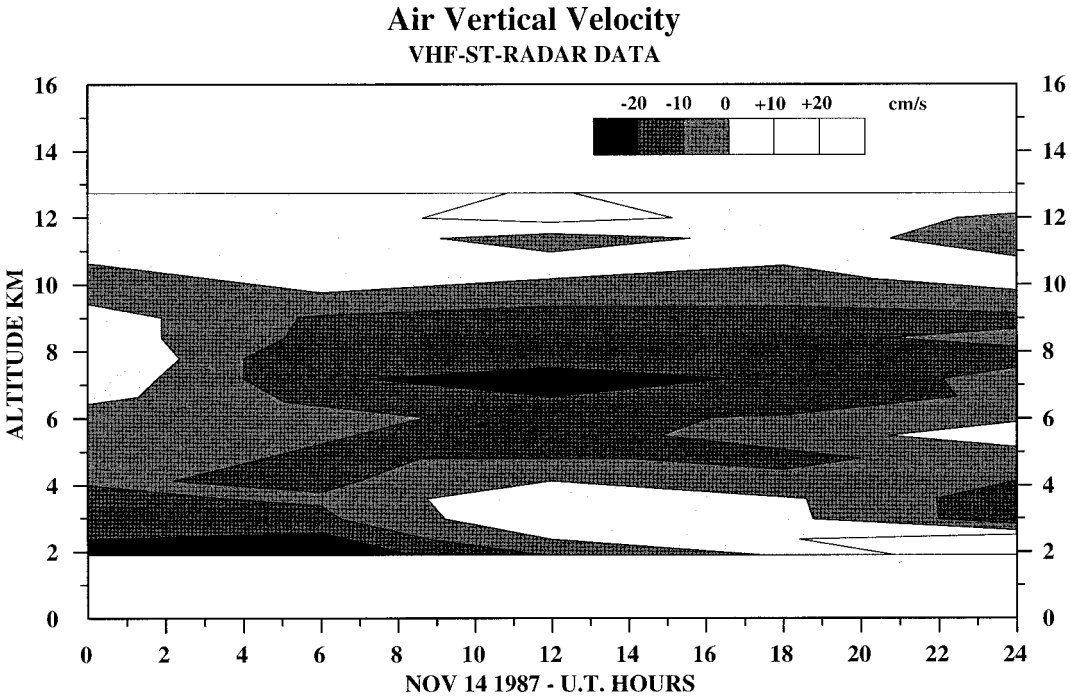

FIG. 18. Same as Fig. 16 but for vertical velocity obtained from 6-h-averaged radar data.

comparison allows us to conclude that, at least for timescales of 6 h, the vertical velocity estimated by the radar and that calculated by the ECMWF model are consistent in the vicinity of the upper-level frontal zone. From a geophysical viewpoint, and as expected, the air is found to be subsident nearby the upper-level frontal zone passage. Maximum subsidence values of -27 cm s^{-1}, at 1200 UTC and 7800-m altitude, and -28 cm s^{-1}, at 1200 UTC and 8400-m altitude, are found using the radar measurements and the ECMWF calculations, respectively. At 1200 UTC, both those altitudes concern air masses vertically ranging between the frontal surface, at 6600 m, and the lower limit of the jet core, at 9000 m. Now, at the same time and heights, the west–east wind components obtained by the radar and by the ECMWF analyses are, respectively, 27 and 32 m s^{-1}, which means that the air moves downward following a slope of 0.6° from the radar data and 0.5° from the ECMWF data. Both those results are rather consistent with the slope of the upper-level frontal surface of 0.3° previously found.

6. Summary of the results and their implications

A VHF-ST radar method of detection of stable air layers down to the low troposphere was developed and tested on a case study of an upper-level front passage. Diagnoses derived from the ECMWF analyses show that the upper-level frontal zone propagates at a fixed velocity without evolving much during the period studied so that time-to-space radar data conversion are allowed for synoptic interpretations. The slope of the upper-level frontal zone derived from synoptic radiosounding stations (0.3°) was consistently compared with a radar-derived estimation. The radar parameter used is the aspect ratio, that is, the vertical-to-oblique echo power ratio. Consistent interpretations of the time series of the aspect ratio, the turbulence intensity (C_N^2), and the vertical shear magnitude of the horizontal wind, as well as the static stability derived from ECMWF analyses, are made to describe the tropopause break, the slope, and the turbulence associated with the upper-level frontal zone. It is shown that the determination of the VHF radar vertical reflectivity enhancements remains the most reliable method to detect stable air masses above 8-km height and that the aspect-ratio method makes possible stable air detection in the lower troposphere. A direct application of the method in this case study is to allow us to monitor the upper-level front passage down to 4-km altitude.

Also, the vertical velocity field obtained from VHF-ST radar measurements in the vicinity of the upper-level frontal zone was found to be in agreement with the ECMWF calculations provided that time and length scales of about 6 h and 400 km are considered. Such measurements can then be used to improve the description of the vertical motions involved in an upper-level frontal zone passage provided that the horizontal wind strength is not too strong and that the frontal zone slope, here 0.3°, is much smaller than the radar beam half-width, here 2.75°.

Acknowledgments. The ST radar experiment at Lannion has been supported by the Institut National des Sciences de l'Univers (ATP ''FRONTS 87''). The Programme Atmosphère Moyenne of the same institute has supported the data reduction and the research work. We wish to express our gratitude to M. Crochet for helpful scientific discussions and suggestions.

REFERENCES

Browning, K. A., B. J. Hoskins, P. R. Jonas, and A. J. Thorpe, 1986: European collaboration on atmospheric fronts. *Nature,* **322,** 114–115.

Clough, S. A., 1987: The mesoscale frontal dynamic project. *Meteor. Mag.,* **116,** 32–42.

Crochet, M., 1990: Atmospheric profiler radar. Developments and outstanding questions. *Meteor. Rundsch.,* **42,** 123–136.

——, E. Bazile, and G. Rougier, 1990a: Comparison of thermal advection measurements by clear-air radar and radiosonde techniques. *Radio Sci.,* **25,** 907–915.

——, F. Cuq, F. M. Ralph, and S. V. Venkateswaran, 1990b: Clear air radar observations of the great October storm of 1987. *Dyn. Atmos. Oceans,* **14,** 443–461.

Dalaudier, F., C. Sidi, M. Crochet, and J. Vernin, 1994: Direct evidence of ''sheets'' in the atmospheric temperature field. *J. Atmos. Sci.,* **51,** 237–248.

Ecklund, W. L., D. A. Carter, and B. B. Balsley, 1979: Continuous measurement of upper atmospheric winds and turbulence using a VHF Doppler radar: Preliminary results. *J. Atmos. Terr. Phys.,* **41,** 983–994.

Fisher, C., and F. Lalaurette, 1995a: Meso-beta-scale circulations in realistic fronts. I: Steady basic state. *Quart. J. Roy. Meteor. Soc.,* **121,** 1255–1283.

——, and ——, 1995b: Meso-beta-scale circulations in realistic fronts. II: Frontogenetically forced basic states. *Quart. J. Roy. Meteor. Soc.,* **121,** 1285–1321.

Fukao, S., T. Sato, N. Yamasaki, R. Harper, and S. Kato, 1982: Winds measured by a UHF Doppler radar and rawinsondes: Comparisons made on twenty-six days (August–September 1977) at Arecibo, Puerto Rico. *J. Appl. Meteor.,* **21,** 1357–1363.

Gage, K. S., and B. B. Balsley, 1978: Doppler radar probing of the clear atmosphere. *Bull. Amer. Meteor. Soc.,* **59,** 1074–1093.

——, and J. L. Green, 1978: Evidence for specular reflection from monostatic VHF radar observations of the stratosphere. *Radio Sci.,* **13,** 991–1001.

——, and B. B. Balsley, 1980: On the scattering and reflection mechanisms contributing to clear air radar echoes from the troposphere, stratosphere, and mesosphere, *Radio Sci.,* **15,** 243–257.

Gidel, L. T., and M. A. Shapiro, 1979: The role of clear air turbulence in the production of potential vorticity in the vicinity of jet-stream–frontal systems. *J. Atmos. Sci.,* **36,** 2125–2138.

Green, J. L., and K. S. Gage, 1980: Observations of stable layers in the troposphere and stratosphere using VHF radar. *Radio Sci.,* **15,** 395–405.

——, T. E. VanZandt, W. L. Clark, J. M. Warnock, and G. D. Nastrom, 1988: Observations of vertical velocity over Illinois by the Flatland radar. *Geophys. Res. Lett.,* **15,** 269–272.

Hocking, W. K., S. Fukao, T. Tsuda, M. Yamamoto, T. Sato, and S. Kato, 1990: Aspect sensitivity of stratospheric VHF radio wave scatterers, particularly above 15-km altitude. *Radio Sci.,* **25,** 613–627.

Hoskins, B. J., M. E. McIntyre, and A. W. Robertson, 1985: On the

use and significance of isentropic potential vorticity maps. *Quart. J. Roy. Meteor. Soc.,* **111,** 877–946.

Keyser, D., and M. A. Shapiro, 1986: A review of the structure and dynamics of the upper-level frontal zones. *Mon. Wea. Rev.*, **114,** 452–499.

Larsen, M. F., and J. Röttger, 1982: VHF and UHF Doppler radars as tools for synoptic research. *Bull. Amer. Meteor. Soc.,* **63,** 996–1008.

——, and ——, 1985: Observations of frontal zone and tropopause structures with a VHF Doppler radar and radiosondes. *Radio Sci.,* **20,** 1223–1232.

——, and ——, 1991: VHF radar measurements of in-beam incidence angles and associated vertical-beam radial velocity corrections. *J. Atmos. Oceanic Technol.,* **8,** 477–490.

——, ——, and T. S. Dennis, 1988: A comparison of operational analyses and VHF wind profiler vertical velocities. *Mon. Wea. Rev.,* **116,** 48–59.

——, S. Fukao, O. Aruga, M. D. Yamanaka, T. Tsuda, and S. Kato, 1991: A comparison of VHF radial vertical-velocity measurements by a direct vertical-beam method and by a VAD technique. *J. Atmos. Oceanic Technol.,* **8,** 766–776.

Lott, F., 1995: Comparison between the orographic response of the ECMWF model and the PYREX 1990 data. *Quart. J. Roy. Meteor. Soc.,* **121,** 1323–1348.

Luce, H., M. Crochet, F. Dalaudier, and C. Sidi, 1995: Interpretation of VHF ST radar vertical echoes from in situ temperature sheet observations. *Radio Sci.,* **30,** 1003–1025.

——, F. Dalaudier, M. Crochet, and C. Sidi, 1996: Direct comparison between in situ and VHF oblique radar measurements of refractive index spectra: a new successful attempt. *Radio Sci.,* **31,** 1487–1500.

May, P. T., M. Yamamoto, S. Fukao, T. Sato, S. Kato, and T. Tsuda, 1991: Wind and reflectivity fields around fronts observed with a VHF radar. *Radio Sci.,* **26,** 1245–1249.

Nastrom, G. D., W. L. Ecklund, and K. S. Gage, 1985: On the direct measurement of large-scale vertical velocities using clear-air Doppler radars. *Mon. Wea. Rev.*, **113,** 708–718.

——, W. L. Clark, K. S. Gage, T. E. VanZandt, J. M. Warnock, R. Creasey, and P. M. Pauley, 1994: Case studies of the vertical velocity seen by the Flatland radar compared with indirectly computed values. *J. Atmos. Oceanic Technol.,* **11,** 14–21.

Neiman, P. J., and M. A. Shapiro, 1989: Retrieving horizontal temperature gradients and advections from single-station wind profiler observations. *Wea. Forecasting,* **4,** 222–233.

——, P. T. May, and M. A. Shapiro, 1992: Radio acoustic sounding system (RASS) and wind profiler observations of lower- and midtropospheric weather system. *Mon. Wea. Rev.,* **120,** 2298–2313.

O'Brien, J. J., 1970: Alternative solutions to the classical vertical velocity problem. *J. Appl. Meteor.,* **9,** 197–203.

Redelsperger, J.-L., and J.-P. Lafore, 1994: Non-hydrostatic simulations of a cold front observed during the FRONTS 87 experiment. *Quart. J. Roy. Meteor. Soc.,* **120,** 519–555.

Röttger, J., 1979: VHF radar observations of a frontal passage. *J. Appl. Meteor.,* **18,** 85–91.

——, 1980: Reflection and scattering of VHF radar signals from atmospheric refractivity structures. *Radio Sci.,* **15,** 259–276.

——, and C. H. Liu, 1978: Partial reflection and scattering of VHF radar signals from the clear air atmosphere. *Geophys. Res. Lett.*, **5,** 357–360.

Sortais, J.-L., J.-P. Cammas, X. D. Yu, E. Richard, and R. Rosset, 1993: A case study of coupling between low- and upper-level jet-front systems: Investigation of dynamical and diabatical processes. *Mon. Wea. Rev.,* **121,** 2239–2253.

Strauch, R. G., B. L. Weber, A. S. Frisch, C. G. Little, D. A. Merritt, K. P. Moran, and D. C. Welsh, 1987: The precision and relative accuracy of profiler wind measurements. *J. Atmos. Oceanic Technol.,* **4,** 563–571.

Tennekes, H., and J. L. Lumley, 1972: *A First Course in Turbulence.* MIT Press, 300 pp.

Thorpe, A. J., and S. A. Clough, 1991: Mesoscale dynamics of cold fronts: Structures described by dropsoundings in FRONTS 87. *Quart. J. Roy. Meteor. Soc.,* **117,** 903–941.

——, S. T. Garner, and J. Testud, 1987: Theoretical aspects of the project ''Mesoscale Frontal Dynamical Project.'' Rep. 33, 24 pp. [Available from A. J. Thorpe, JCMM Pitt Building, University of Reading, White Kings Road, P.O. Box 240, Reading RG62FN, United Kingdom.]

Tsuda, T., T. Sato, K. Hirose, S. Fukao, and S. Kato, 1986: MU radar observations of the aspect sensitivity of backscattered VHF echo power in the troposphere and lower stratosphere. *Radio Sci.,* **21,** 971–980.

van Baelen, J. S., A. D. Richmond, T. Tsuda, S. K. Avery, S. Kato, S. Fukao, and M. Yamamoto, 1991: Radar interferometry technique and anisotropy of the echo power distribution: First results. *Radio Sci.,* **26,** 1315–1326.

Yoe, J. G., and R. Rüster, 1992: VHF Doppler radar observations of vertical velocities in the vicinity of the jet stream. *Mon. Wea. Rev.,* **120,** 2378–2382.

——, P. Czechowsky, R. Rüster, and G. Schmidt, 1994: Spatial variability of the aspect sensitivity of VHF radar echoes in the troposphere and lower stratosphere during jet stream passages. *Ann. Geophys.,* **12,** 733–745.